J. Fluid Mech. (1979), *vol.* 94, *part* 3, *pp.* 453–463
Printed in Great Britain

Marginal instability in Taylor–Couette flows at a very high Taylor number

By A. BARCILON,
Geophysical Fluid Dynamics Institute, Florida State University
J. BRINDLEY,
Department of Applied Mathematical Studies, University of Leeds
M. LESSEN
Department of Mechanical and Aerospace Sciences, University of Rochester
AND F. R. MOBBS
Department of Mechanical Engineering, University of Leeds

(Received 24 October 1978)

We report on a set of turbulent flow experiments of the Taylor type in which the fluid is contained between a rotating inner circular cylinder and a fixed concentric outer cylinder, focusing our attention on very large Taylor number values, i.e.

$$10^3 \leqslant T/T_c \leqslant 10^5,$$

where T_c is the critical value of the Taylor number T for onset of Taylor vortices. At such large values of T, the turbulent vortex flow structure is similar to the one observed when $T - T_c$ is small and this structure is apparently insensitive to further increases in T. These flows are characterized by two widely separated length scales: the scale of the gap width which characterizes the Taylor vortex flow and a much smaller scale which is made visible by streaks in the form of a 'herring-bone'-like pattern visible at the walls. These are conjectured to be Görtler vortices which arise as a result of centrifugal instability in the wall boundary layers. Ideas of marginal instability by which we postulate that both the Taylor and Görtler vortex structures are marginally unstable on their own scale seem to provide good quantitative agreement between predicted and observed Görtler vortex spacings.

1. Introduction

In this paper we present the results of experiments by one of us (F. R. Mobbs) and attempt to explain some of the novel features of the results for large values of the non-dimensional parameter which characterizes these flows. The experiments examine the behaviour of a fluid contained between two concentric circular cylinders when the inner cylinder rotates, whilst the outer one remains fixed. The basic problem is known as the Taylor–Couette problem in recognition of the important original experiments performed and the theory proposed by Taylor (1923) and it is certainly one of the best-known problems in the whole field of fluid mechanics; indeed, it is so well documented as to be a useful testing ground for many new techniques, both theoretical and

0022-1120/79/4246-7250 $02.00

T/T_c	Wavenumber	Remarks
1·03	—	Internal waves
1·08	—	Waviness of out-going jets visible at outer cylinder
1·24	3	Waviness of all Taylor cell boundaries commences
1·70	4	—
1·92	5	—
2·28	6	—
2·83	7	Changes in azimuthal wavenumber occur at unique values of T/T_c. Harmonics and secondary wavenumbers are weak
4·65	8	—
5·59	9	—
16·9	10	—
16·9–19·3	10–9	Predominant wavenumber variable
19·3–73·3	9–5	
73·3	5	Return to stable wavenumbers
102·9	4	
419	—	Transitional stage
445	—	Waviness of cell boundaries replaced by internal waves. Gradual appearance of Görtler vortices
↓		

Results for T/T_c up to about 20 were obtained using H.V.I. 60, those for higher values of T/T_c were obtained using Tellus 13.

TABLE 1. Summary of results using H.V.I. 60 and Tellus 13.

experimental, in an effort to grasp an understanding of the various regimes observed and the break-down to turbulence.

If r denotes the mean radius, Ω the angular velocity of the inner cylinder, d the gap width and ν the kinematic viscosity, the non-dimensional parameter

$$T = r\Omega^2 d^3/\nu^2$$

is of vital importance in determining the flow pattern. As T is increased the following flow sequences are observed: At a critical value T_c of T the flow changes from a Couette motion which is uniform in the axial direction to a Taylor vortex flow in which the gap is completely filled by an array of toroidal vortices. At a higher value T_w of T the toroidal vortices begin to exhibit a wavy structure with waves progressing in the azimuthal direction, the wavenumber increasing for a while with increasing T. The appearance of these non-axisymmetric modes has been comprehensively described by Coles (1965) and numerous other workers, notably Snyder (1970). As T increases further the waviness degenerates into a complex pattern, presumably as a consequence of nonlinear interactions of several wavenumbers present at once. At still higher T the waviness of the Taylor cell boundaries disappears but the evidence both of the slit illumination observations and of spectral measurements suggest the persistence of a low wavenumber disturbance of the cell core. Further increase in the Taylor number does not seem to alter that pattern. It is with the flow at these high Taylor numbers that the present paper is concerned. (The reader is referred to table 1 and figure 1 for a more quantitative description of the above sequence of flow fields.)

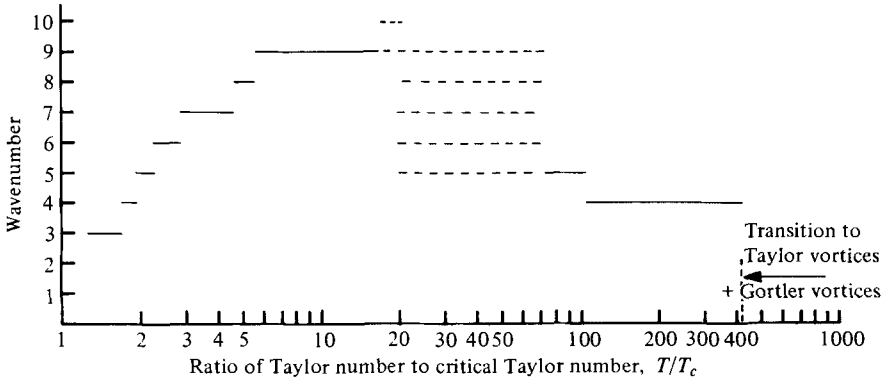

FIGURE 1. Ranges of Taylor number over which particular wavenumbers are observed. ——, unique wavenumber; – – – –, non-unique wavenumber.

In earlier experiments at large T, G. I. Taylor (1935) observed that the mean azimuthal velocity field developed a wide core, in which the circulation was nearly constant, separated from each of the walls by a thin boundary layer in which the velocity adjusted to the appropriate value. Taylor's experiments were conducted for a wide gap while Wattendorf (1935) found the same result for a narrow gap. Both sets of experiments involved conditions appropriate to about 10^3–10^4 times the critical Taylor number T_c.

A second feature of the flow pattern at very high T was first mentioned by Pai (1943) who observed a periodic structure of vortices, similar to the ones observed when $T - T_c$ is small, even though the flow appeared to be highly turbulent. Rather strangely this phenomenon does not appear to have received much attention, presumably because few experiments were carried out at sufficiently large Taylor numbers.

The present observations suggest that these flows exhibit 'turbulence' on two distinct scales: the scale of the gap width which is filled by a 'turbulent' Taylor vortex and a much smaller scale which is indicative of a structured small scale pattern of flow clinging to the walls, this pattern having a herring-bone-like appearance.

We wish to address ourselves to the novel observation at high Taylor number of this very ordered structure which occurs on a scale of motion a good deal smaller than the basic Taylor vortices. The structure is highly suggestive of Görtler vortices found in the boundary layer created by the Taylor vortex circulation. We postulate that the Taylor vortex flow redistributes the mean zonal velocity profile so as to create, near the cylindrical walls, boundary layers of thickness δ in which centrifugal instabilities cause Görtler vortices to form on scale related to δ and this is the scale of the observed herring-bone pattern streaks seen at high T.

In § 4 we argue that the persistence and stability of both Taylor and Görtler vortex structures over a large range of Taylor numbers suggest that each is in a certain sense marginally stable. This concept of marginal stability has already been used by two of us to explain features of the large scale structures in turbulent flows of a geophysical nature (Lessen, Barcilon & Butler 1977; Barcilon & Lessen 1978) and for turbulent jet, wake and shear flows (Lessen & Singh 1974; Lessen & Paillet 1976; Lessen 1978). The flow described in this paper is made more complicated than those found in the works cited above because of the presence of rigid walls, yet it provides an example

in which the geometrical constraints maintain both the large and small scale structures in a remarkably steady form. The extremely good agreement between the predicted and measured Görtler vortex spacing illustrated in figure 7 gives credibility to these ideas.

2. Apparatus and experimental procedure

The apparatus consisted of a pair of co-axial cylinders, the inner cylinder being capable of rotation while the outer cylinder was fixed. Both cylinders were fabricated from rolled acrylic plastic sheet 12·7 mm thick, welded at the joint.

The internal face of the outer cylinder was then machined to a diameter of

$$152{\cdot}5\,\text{mm} \pm 12{\cdot}5\,\mu\text{m}.$$

The inner cylinder was machined to a diameter of 138·5 mm $\pm$ 12·5 μm, giving a radius ratio $R_1/R_2 = 0{\cdot}908$. Rings attached to the outer cylinder determined the annulus length at 915 mm, giving a length to gap ratio of 65. End plates bonded to the inner cylinder were centrally bored to accept a drive shaft and a stub shaft, respectively, the tolerance not exceeding 50 μm. The inner cylinder was mounted with a deep groove ball bearing at each end and the outer ring of each bearing located in radially moveable end plates.

On assembly the inner cylinder was mounted concentric to and aligned with the outer cylinder using dial gauges. Adjustable stops, attached to the outer cylinder, were then located on the inner cylinder, ensuring concentricity and alignment to within 25 μm thereafter. The drive unit was mounted directly above the drive shaft and the speed measured by means of a steel gear wheel, located between the motor and the drive shaft, and a magnetic pick-up connected to a digital counter. The fluid temperature was measured by thermocouples located flush with the outer cylinder wall at three axial positions.

Three fluids were used to achieve a wide range of Taylor numbers. These were H.V.I. 60 (ν = 60·6 cSt at 19·6 °C), Tellus 13 (ν = 18·5 cSt at 20 °C) and kerosene (ν = 1·69 cSt at 19 °C). Some results were also obtained using air.

Flow visualization with the liquids was obtained by employing a suspension of aluminium paint pigment in the test fluid. In addition to front lighting a cross-section of the flow was illuminated using a 2 mm wide axial slit.

The information derived from the visual studies was supplemented by analysing the signals from two DISA fibre film probes, 30° apart, used in conjunction with two DISA M series constant temperature anemometers. The signals were digitized and analysed on-line by a PDP11/70 computer comprising the SRC Interactive Computing Facility at Leeds University.

The total number of digitalized samples was 800 and the sampling rate varied from 100 to 500 samples/s over the Taylor number range. Autocorrelation and cross-correlation functions were calculated directly from the digitalized data and the power spectral density function was determined using a fast Fourier transform. The delay time corresponding to the first maxima on the cross-correlation curve was used to determine the wave speed. Wherever possible this was used to convert the frequency scale of the spectrum to a wavenumber scale. When the wave speed measurement

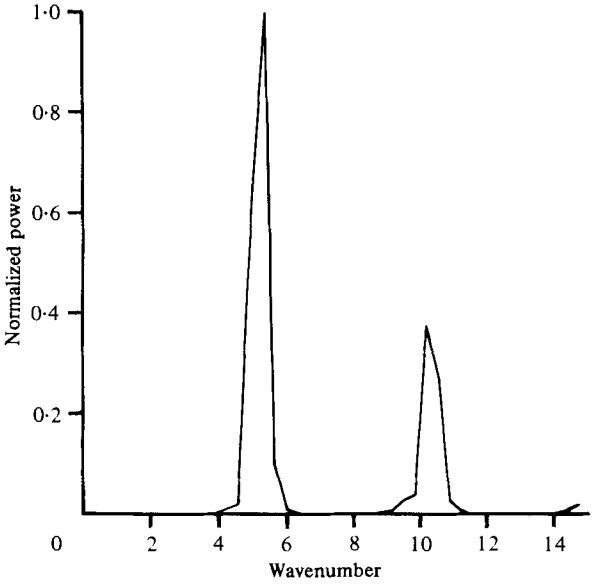

FIGURE 2. Power spectrum obtained from hot-film probe measurements, as described in text, for $T/T_c = 1{\cdot}92$.

became unreliable (at $T > 415\,T_c$) the frequency scale was non-dimensionalized with respect to the inner cylinder speed.

3. Results

Before considering the results for high T it is useful to deal briefly with the sequence of events observed as the Taylor number is slowly increasing from its critical value. These are summarized in table 1 and figure 1.

The first sign of waviness of the Taylor vortices occurs at $T/T_c = 1{\cdot}03$. In the front view this appears as a waviness of the bright bands of aluminium flakes marking the vortex cell centres. The axial slit illumination shows the centre of circulation in each cell to be describing a circular path. The locus of cell centres is therefore, at any instant, a spiral. At this stage the cell boundaries remain unaffected by these internal waves.

The usually reported type of wavy vortex motion in which all the Taylor cell boundaries are wavy does not become established until the Taylor number reaches a value T_w where $T_w/T_c = 1{\cdot}24$ and when the fluid is oil of high viscosity (H.V.I. 60) the azimuthal wavenumber increases from 3 to 10 between $T/T_c = 1{\cdot}24$ and $T/T_c = 16{\cdot}9$ in well-defined stages. The spectra have a single peak, apart from harmonics (figure 2). In contrast, when air is used as the fluid in this Taylor number range the predominant wavenumber is no longer constant. At any Taylor number several wavenumbers of significant magnitude are usually present in the spectrum and the predominant wavenumber varies with time. The H.V.I. 60 and Tellus 13 results show a similar tendency in the range $T/T_c = 16{\cdot}9$ to $T/T_c = 73{\cdot}3$, where the predominant wavenumber varies between 10 and 5, but in general the wavenumber falls with increasing Taylor number (figure 3).

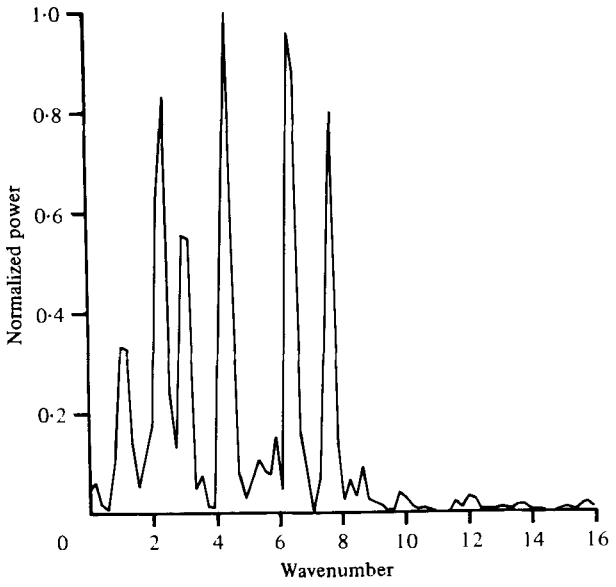

FIGURE 3. Power spectrum obtained from hot-film probe measurements as described in text, for $T/T_c = 20{\cdot}0$.

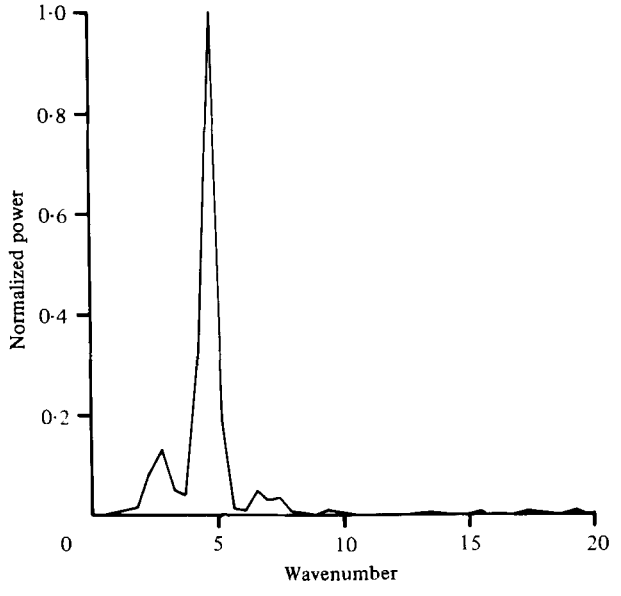

FIGURE 4. Power spectrum obtained from hot-film probe measurements, as described in text, for $T/T_c = 73{\cdot}4$.

Broadly similar results, based on visual observations, have been obtained by Short & Jackson (1977), but the viscosity of their fluid (a mineral oil) is not stated.

A stable wavenumber regime with 5 waves is again established at $T/T_c = 73{\cdot}3$ (figure 4), followed by a transition to 4 waves at $T/T_c = 102{\cdot}9$. The stable wavenumber regime ends at $T/T_c = 419$. Swinney, Fenstermacher & Gollub (1977) have also

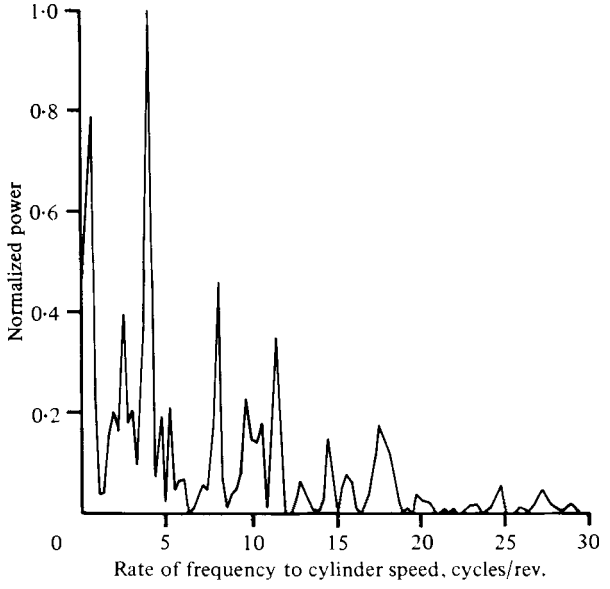

FIGURE 5. Power spectrum obtained from hot-film probe measurements, as described in text, for $T/T_c = 23400$.

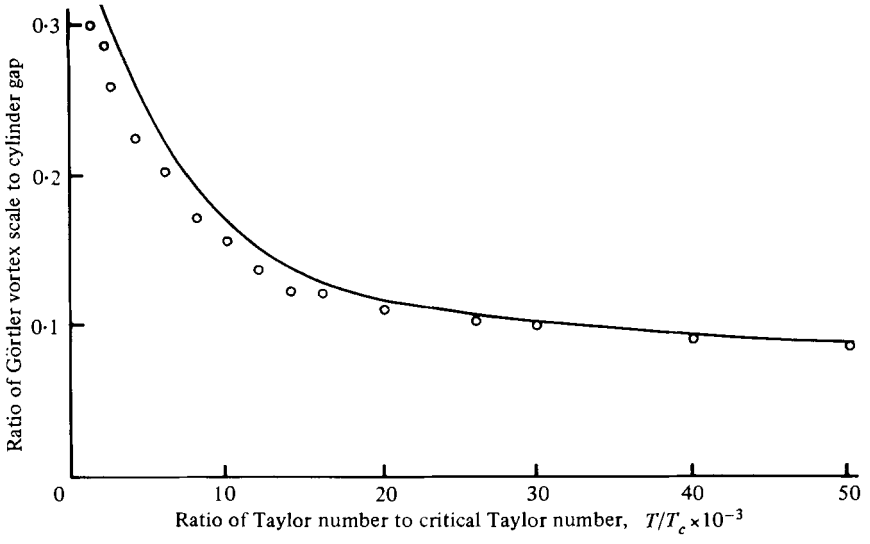

FIGURE 7. Observations of streak width shown by ⊙; Görtler vortex width $\lambda_G/2$, given by equation (4.6), shown by solid line.

reported a 4 wave regime which ends at about $T/T_c = 497$, for a radius ratio of 0·877. Subsequently there is a gradual transition to a state of motion in which waviness of the Taylor cell boundaries is absent, but an oscillation of the vortex cell centres, indicating internal waviness, can be seen by axial slit illumination. These internal waves are believed responsible for a number of low frequency spectral peaks which are, however, in a state of rapid change. A number of higher frequency peaks also

appear in the spectra (figure 5), not all of which can be identified as harmonics of the predominating lower frequencies. At the same time photographic evidence shows the gradual emergence of a well-defined series of parallel streaks superimposed on the Taylor cells, which we believe to be due to Görtler vortices.

It is with this last, high Taylor number regime that we are primarily concerned. Examination of the photographs, figure 6 (plate 1), enables the average scale of the Görtler vortices to be determined and this is shown plotted against T/T_c in figure 7.

4. Discussion

The principal features of the flow behaviour have been summarized in table 1. A number of features are particularly noteworthy; at small values of $T-T_c$, when $T < T_w$, visual observations show that the *core* of the Taylor vortex has a wavy disturbance of low wavenumber even when the boundaries of the Taylor cells at the cylindrical walls are straight. When T exceeds T_w wavy disturbances become visible at the walls, and at these values of T spectral observations detect a low frequency component in the core identifiable with the visible waves. (See e.g. figure 2 at

$$T/T_c \sim 1{\cdot}92,$$

at which value a wavenumber 5 is predominant.) Since $T_w - T_c \ll T_c$ for small gap, the existence of a low frequency perturbation of the core, while the cell boundaries remain unperturbed, might be taken as an indicator of a state near to marginal stability for the Taylor vortices. We return to this point later.

The spectral measurements also show a qualitative change at $T/T_c \sim 400$; for lower values the spectrum is very 'clean', with prominent peaks identifiable as the wavy modes affecting the boundary (figure 4); for higher values a substantial high frequency element is present (figure 5), which is presumably a measure of small scale motion in the interior on a scale compatible with the Görtler cells. At a similar value of the Taylor number the visible waviness of the cell boundaries dies out, but the spectral measurements and illuminated slit observations still indicate a large amplitude low frequency mode in the interior identical with that observed in the visually wavy regime. Comparison with T slightly greater than T_c suggests that we are again reaching a state of near marginal stability for the basic Taylor vortices. However, the flow within these vortices is characterized by a substantial small scale fluctuation intensity, whose effect on momentum transport near the boundary is akin to that produced by a much larger viscosity – analogous to the concept of an eddy viscosity used to model transport processes in a turbulent flow. As the Taylor number increases the scale of the Görtler cells decreases and figure 7 presents some results; the amplitude is impossible to observe directly.

But the striking feature of the flow patterns for increasing T/T_c from about 400 on upwards to at least 80000, in other words over a range spanning a factor of 200 in Taylor number, is the stability of the form of the visible Taylor cells; no large scale waviness appears at the boundary despite the existence in the interior of low frequency disturbances of substantial amplitude, and this leads us to our basic proposal concerning the mechanics of the motion, namely that the small scale motion illustrated by the herring-bone pattern of streaks and the large scale motion embodied in the Taylor cells interact so that each of them is a marginally unstable disturbance to the

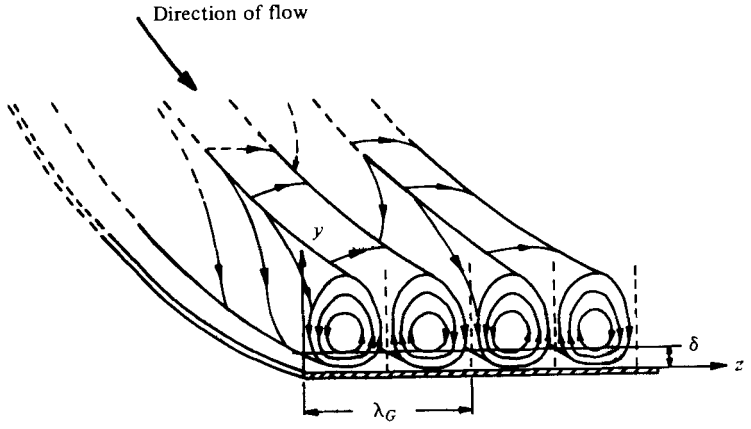

FIGURE 8. Schematic diagrams of Görtler vortices on a concave wall.

basic flow on the scale that it 'sees', the streaks on the boundary-layer scale, the Taylor vortices on the whole gap width.

It is worth recalling the essential dynamics of the Görtler vortices which we propose as the cause of the streaks seen in photographs and films of the motion at very high Taylor numbers. They result from a 'centrifugal instability', closely related to that producing the Taylor vortices, of a curved flow in which the circulation decreases outwards, which produces an array of vortices aligned with the mainstream flow as shown in figure 8 after Görtler (1940). Görtler's analysis of the problem of viscous flow along a concave boundary indicated the critical importance of a parameter

$$G = \left(\frac{U_0 \delta}{\nu}\right)^2 \frac{\delta}{r_c} \tag{4.1}$$

in determining the character of the flow; for values of G above a critical value G_c the spanwise uniform flow is replaced by an array of 'Görtler' vortices. Here U_0 is mainstream velocity, δ is boundary-layer thickness, and r_c the radius of curvature of the boundary.

If we interpret the boundary-layer thickness δ to be the momentum thickness δ_2, defined by

$$\delta_2 = \int_0^\infty \frac{u}{U_0}\left(1 - \frac{u}{U_0}\right) dy,$$

then the minimum critical value of G is near 0·09, and Hammerlin (1956) pointed out that, if δ/r_c is small, this minimum critical value of G occurs for a wavelength large compared with δ. The value 0·09 is fairly insensitive to the exact shape of the boundary-layer profile and the critical wavelength λ_G for $\delta/r_c \sim 10^{-4}$ was shown by Hammerlin to be near $40\pi\delta_2$; for larger δ/r_c this wavelength will be somewhat less.

In figure 7 we have summarized the variation of the streak width as T varies. Since the wavelength λ_G associated with the Görtler vortices covers a pair of counter-rotating vortices, we should identify this streak width with $\frac{1}{2}\lambda_G$, i.e. approximately $20\pi\delta_2$. But since

$$G = \left(\frac{U_0 \delta_2}{\nu}\right)^2 \frac{\delta_2}{r_c}$$

we have

$$\delta_2 = \left(\frac{G\nu^2 r_c}{U_0^2}\right)^{\frac{1}{3}}, \tag{4.2}$$

and if we set $U_0 = \frac{1}{2} r_1 \Omega$, which is approximately true for the mean velocity profile observed in a narrow gap situation, then

$$G = \frac{r_1^2 \Omega^2 \delta_2^3}{4\nu^2 r_c} = \frac{T}{4}\left(\frac{\delta_2}{d}\right)^3 \frac{r_1}{r_c}. \tag{4.3}$$

Thus if we set $G = G_c = 0{\cdot}09$ we have

$$\frac{\delta_2}{d} = \left(\frac{0{\cdot}36}{T}\frac{r_c}{r_1}\right)^{\frac{1}{3}} \tag{4.4}$$

and the streak width

$$\tfrac{1}{2}\lambda_G = 20\pi\delta_2 = 20\pi d\left(\frac{0{\cdot}36}{T}\frac{r_c}{r_1}\right)^{\frac{1}{3}}. \tag{4.5}$$

The value of r_c of course depends on the orientation of the Görtler vortices, but for the observed small angles of deviation from the orientation of the Taylor vortices $(r_c/r_1)^{\frac{1}{3}}$ is quite near unity and hence we can write

$$\tfrac{1}{2}\lambda_G \sim 20\pi d \times 0{\cdot}7 \times (T)^{\frac{1}{3}}. \tag{4.6}$$

The solid line on figure 7 illustrates the value of $\frac{1}{2}\lambda_G$ given by (4.6), and the closeness of fit is remarkable especially when one recognizes that the correction for the value of δ/r_c, slightly larger than 10^{-4} in the experiment (more like 3×10^{-4}), will lead to a slightly smaller factor than the 20π in (4.6).

We have already remarked that a prominent feature of the spectral analyses described in paragraph 3 is the marked changeover from a 'clean' appearance having a small number of definite peaks to a form in which there is much more energy associated with larger wavenumbers. This changeover always takes place at a value of T/T_c near 400, and a similar phenomenon has been observed by Gollub & Swinney (1975) at a comparable value of T/T_c. It is interesting that this value of T/T_c corresponds to a value of $\frac{1}{2}d$ for the Görtler vortex diameter, in other words the maximum diameter compatible with the existence in a stable form of spiral Görtler vortices circumscribing the Taylor vortices.

Below this value of T/T_c, the Görtler vortices presumably interfere with each other in the core region of the Taylor vortex, or perhaps it would be more accurate to say that the conditions have been violated under which it is reasonable to regard the stability of the boundary layer on one cylindrical wall in isolation from the effect of the presence of the other wall.

In summary then, these experiments at high T provide a situation in which a 'turbulent' flow nevertheless is ordered and steady to a remarkable degree. The motion is concentrated in two distinct scales, each of which is clearly distinguishable and related to a primary instability mode of a marginally unstable flow, namely the Taylor vortices of the main channel width and the Görtler vortices of the boundary layer.

Many other instances of turbulent flow indicate a similar coexistence of large scale and small scale eddies, rather than a continuous spectrum of eddy sizes, and it may well be that the highly ordered structure of turbulent flow in these concentric cylinder

experiments could provide a testing ground for elementary theories of turbulence; towards this end a full mathematical treatment of the relationship between the Taylor and Görtler cell amplitudes, and of the energy fluxes between the mean flow and the Taylor and Görtler scales of motion forms the basis of a subsequent paper.

REFERENCES

Barcilon, A. & Lessen, M. 1978 *Tellus* **30**, 557–562.

Coles, D. 1965 *J. Fluid Mech.* **21**, 385–425.

Gollub, J. P. & Swinney, H. L. 1975 *Phys. Rev. Lett.* **35**, 927.

Görtler, H. 1940 *Nachr. Ges. Wiss. Göttingen, Maths. Phys. Kl.* **1**, 1–26 (translated as *N.A.C.A. Tech. Mem.* no. 1375).

Hammerlin, G. 1956 *Z. angew. Math. Phys.* **7**, 156–164.

Lessen, M. 1978 *J. Fluid Mech.* **88**, 535–540.

Lessen, M., Barcilon, A. & Butler, T. E. 1977 *J. Fluid Mech.* **82**, 449–454.

Lessen, M. & Singh, P. J. 1974 *Phys. Fluids* **17**, 1329–1331.

Lessen, M. & Paillet, F. L. 1976 *Phys. Fluids* **19**, 942–945.

Pai, S. I. 1943 *N.A.C.A. Tech. Note* no. 892.

Short, M. G. & Jackson, J. H. 1977 In *Superlaminar Flow in Bearings, Proc. 2nd Leeds–Lyon Symp. Tribology* (ed. D. Dowson, M. Godet and C. M. Taylor), pp. 28–33. Lond. Inst. of Mech. Eng.

Snyder, H. A. 1970 *Int. J. Non-linear Mech.* **5**, 659–685.

Swinney, H. L., Fenstermacher, P. R. & Gollub, J. P. 1977 In *Synergetics* (ed. H. Haken), pp. 60–69. Springer.

Taylor G. I. 1923 *Phil. Trans. Roy. Soc.* A **223**, 289–343.

Taylor, G. I. 1935 *Proc. Roy. Soc.* A **151**, 494–512.

Wattendorf, F. L. 1935 *Proc. Roy. Soc.* A **148**, 565–598.

(*a*)

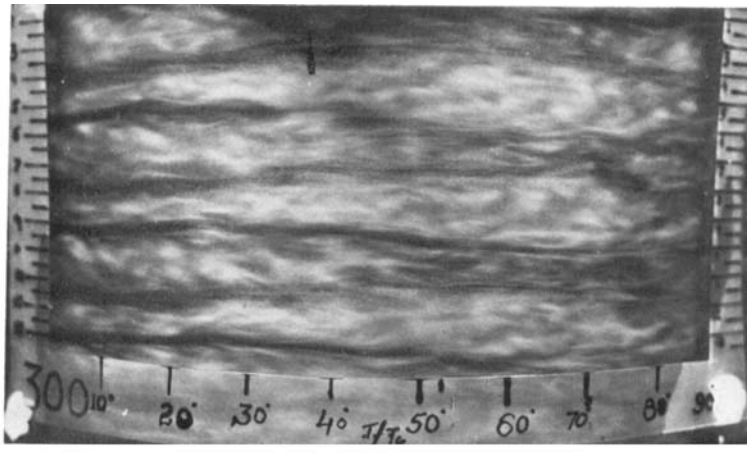

(*b*)

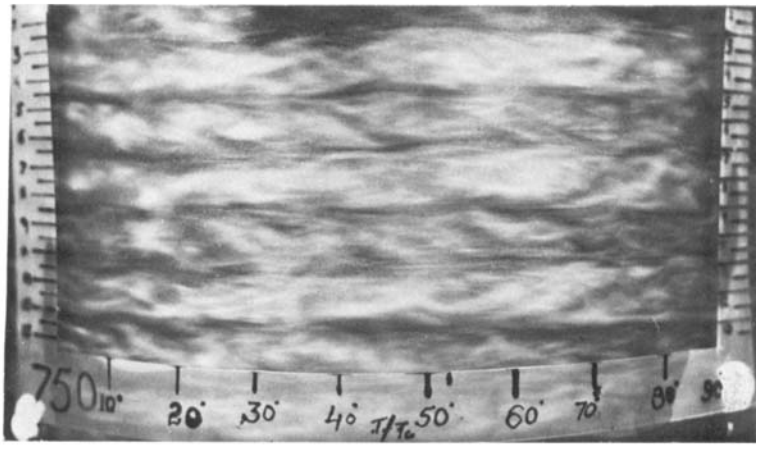

(*c*)

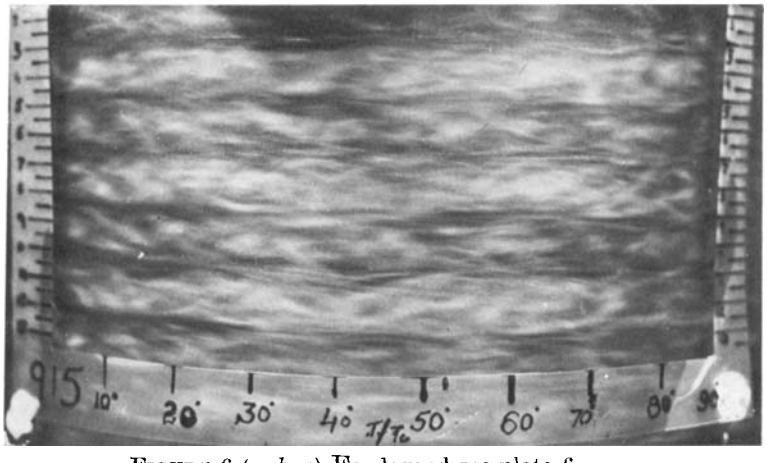

FIGURE 6 (*a*, *b*, *c*) For legend see plate 6.

(*d*)

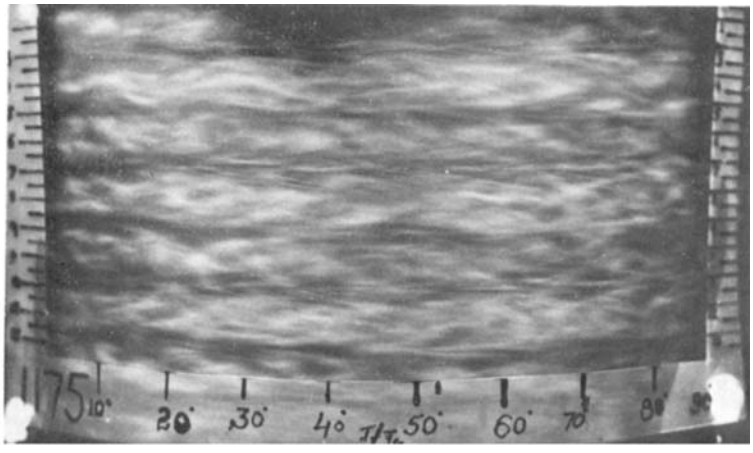

(*e*)

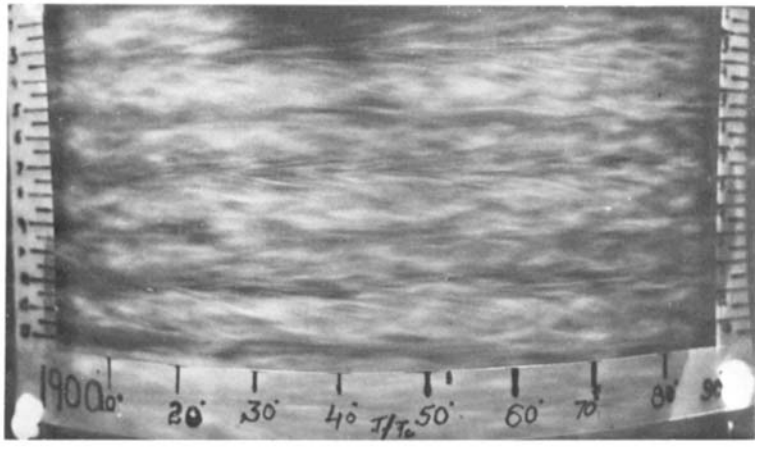

(*f*)

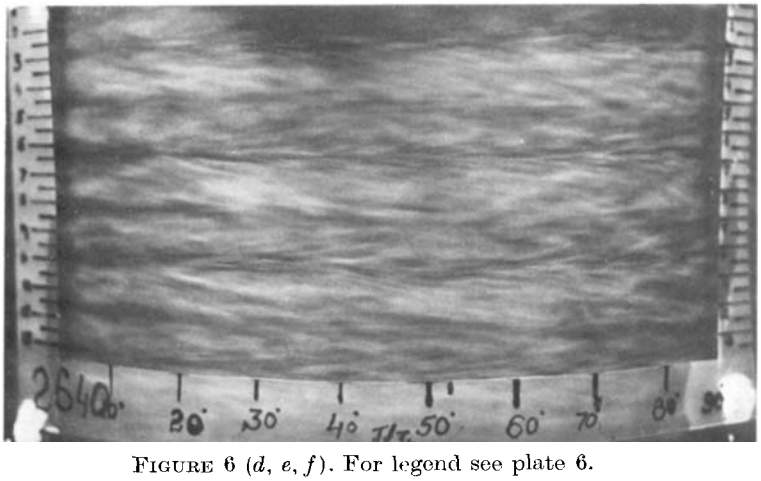

FIGURE 6 (*d*, *e*, *f*). For legend see plate 6.

(*g*)

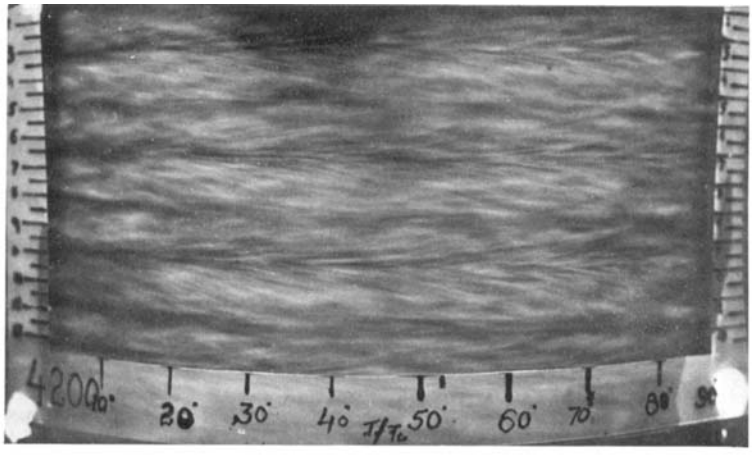

(*h*)

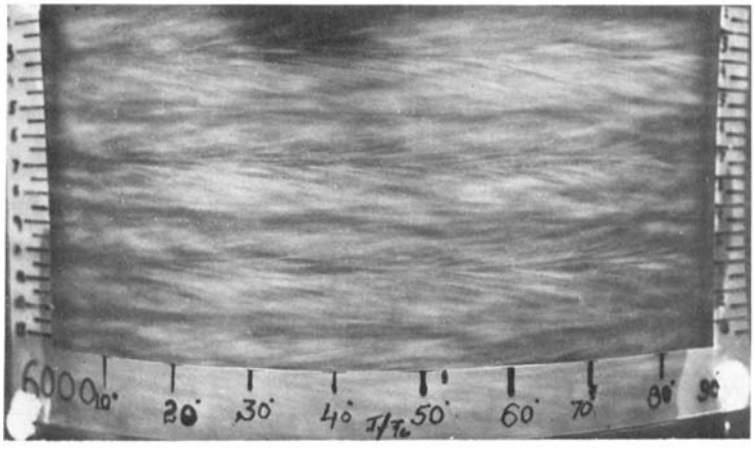

(*i*)

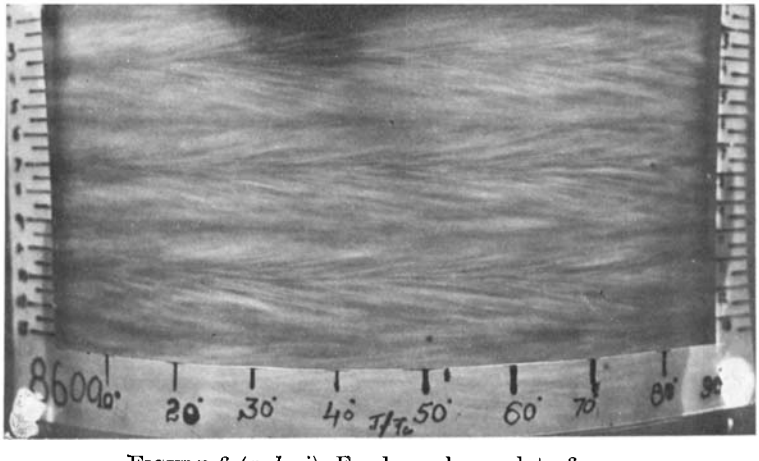

FIGURE 6 (*g*, *h*, *i*). For legend see plate 6.

(*j*)

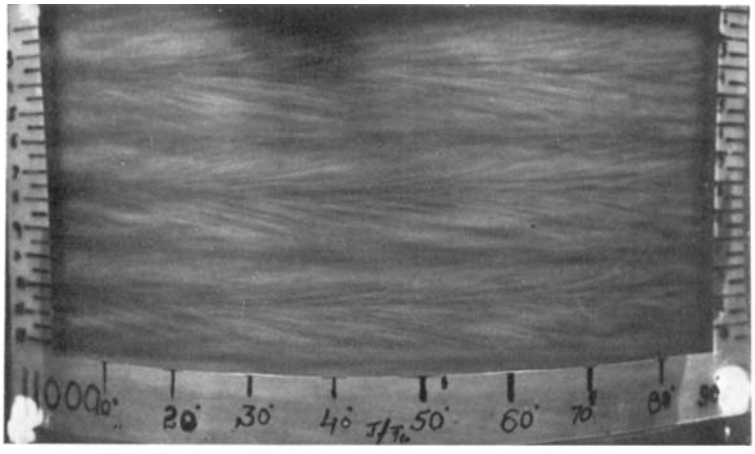

(*k*)

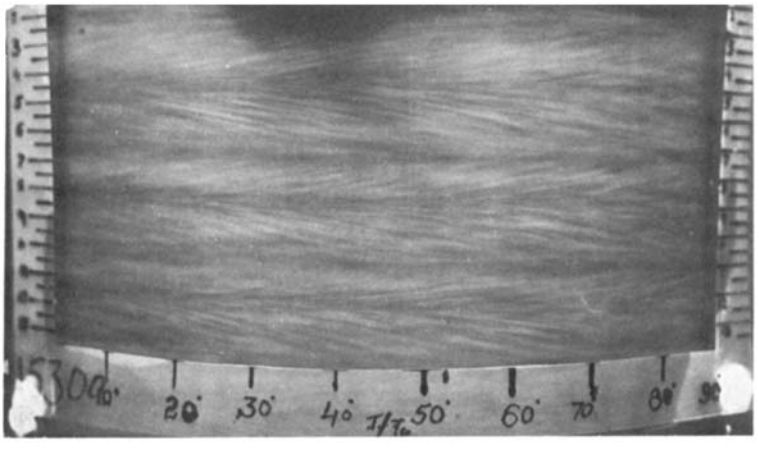

(*l*)

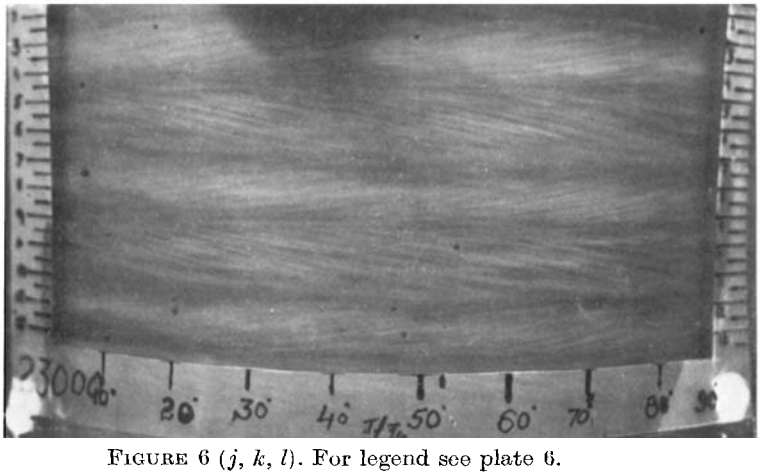

FIGURE 6 (*j*, *k*, *l*). For legend see plate 6.

(*m*)

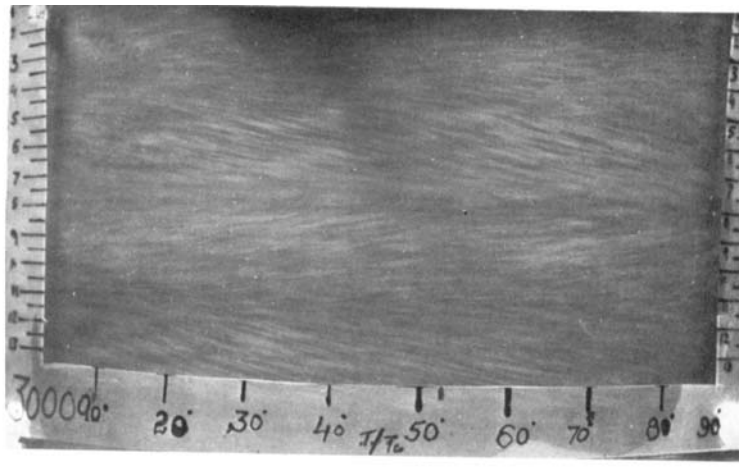

(*n*)

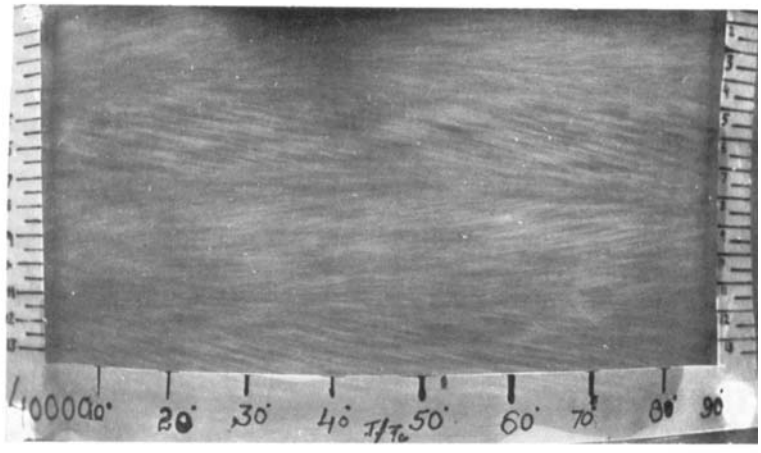

(*o*)

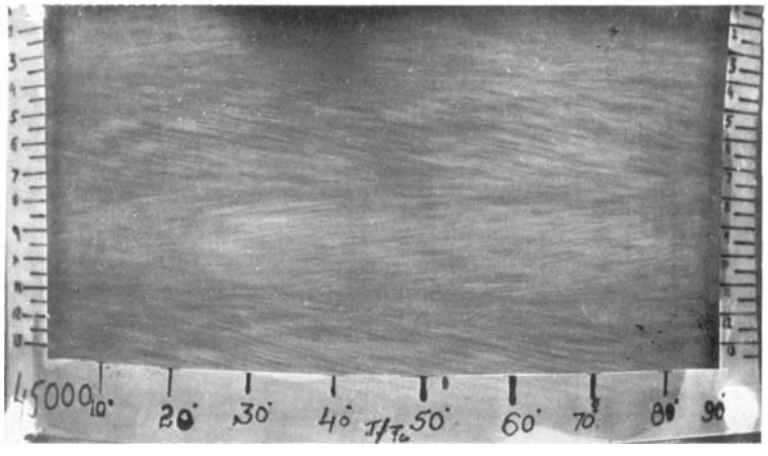

FIGURE 6 (*m*, *n*, *o*). For legend see plate 6.

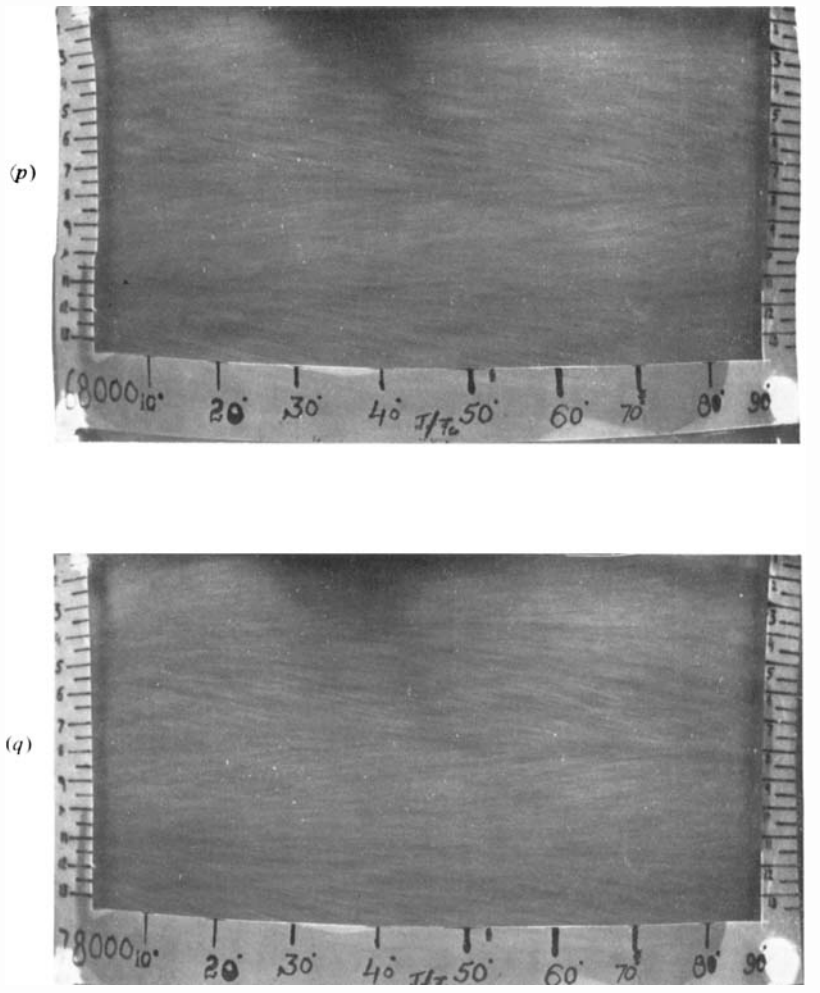

FIGURE 6. Front view photographs of the flow at a range of values of T/T_c. (*a*) 300; (*b*) 750; (*c*) 915; (*d*) 1175; (*e*) 1900; (*f*) 2640; (*g*) 4200; (*h*) 6000; (*i*) 8600; (*j*) 11000; (*k*) 15300; (*l*) 23000; (*m*) 30000; (*n*) 40000; (*o*) 45000; (*p*) 68000; (*q*) 78000.